Design, modeling and fabrication of low cost and miniaturized optical engine based on organic optical bench

JUAN WEI[a,b,c], FENGMAN LIU[a,b,*], HAIYUN XUE[a,b,*], FENGZE HOU[a,b], HUIMIN HE[a,b], YU SUN[a,b], SIWEI SUN[a,b], ZHIXIONG LI [a,b,c], LIQIANG CAO[a,b]

[a]*System Packaging and Integration Research Center, Institute of Microelectronics of Chinese Academy of Sciences, Beijing 100029, China*
[b]*Beijing Key Laboratory of New Generation Communication RF Technology, Institute of Microelectronics of Chinese Academy of Sciences, Beijing 100029, China*
[c]*University of Chinese Academy of Sciences, Beijing 100049, China*

A low-cost and small-scale optical engine using passive direct coupling method based on organic substrate technology is proposed and demonstrated in this paper. The design and fabrication of the organic optical bench (OOB) including analysis on optical coupling efficiency and electrical 3-dB bandwidth and fabrication process of organic optical bench is firstly presented. Then the properties of organic substrate are tested. Thermal cycle analysis and vibration are modeled and simulated as well. The simulation results show that stress and strain have little effect on the coupling efficiency and the golden bump joint has good reliability. Finally, the whole optical subsystem assembly process flow is introduced and the corresponding test system is built to verify the performance of the optical engine. Test results show the optical eye diagrams of the four-channel transmitters and electrical eye diagrams of the four-channel receivers are all clearly open enough to support standard 10Gbps data rate. Organic substrate material is seldom studied and applied for optical carrier before, the optical engine proposed in this paper demonstrated its feasibility and potential to be applied in short-reach optical interconnection and high speed applications such as video/audio signals transmission.

1. Introduction

Starting ten to fifteen years ago, ever-increasing bandwidth demand in the data centers created a need for extensive fiber interconnection deployment. Now, due to the rapidly rising demand for large capacity transmission of video/audio signals, similar trends in optical interconnection among consumers have attracted amount of attention. The interface data rates of Thunderbolt, USB, and HDMI is also increasing quickly. For example, Thunderbolt3 officially runs on copper cables up to 0.8 meters [1]. As a result, optical interconnection has become a viable alternative to conventional copper-based cables which pose several critical issues on structures and systems in terms of bandwidth, electromagnetic interference, weight and thermal management.

The availability of low-cost optical subassembly modules (OSAs) is essential to accelerating the penetration of optical interconnection into the consumer market, which can be realized by two approaches. One is primarily reducing the cost of optical sources and connecting fibers. Besides, trying to make assembly procedures easier is a feasible method [2-4]. As key technology of OSA, optical engine has been widely studied for its critical effects on performance of OSA and its high-proportioned cost in whole modules. Researchers have tried to implement optical engines based on various benches. Chen [5] and Feng [6] proposed an optical engine based on silicon optical bench. Park [7] and Mathew [8] proposed an optical engine based on ceramic substrates. In addition, printed circuit board (PCB) has been widely used in chip on board (CoB) package and non-hermetic package [9,10]. Organic substrate material, which has the advantages of mature process, larger panel size and low cost, has been widely used in electrical packaging. However, it is seldom studied and applied for optical engine.

In this paper, an optical engine using passive direct coupling method based on organic optical bench (OOB) is designed and implemented. Wire bonding, flip-chip and panel level process are chosen as assembly methods to achieve optical coupling since they are mature and costless. This paper is organized as follows. In Section 2, design of the optical engine based on OOB and its fabrication process are described in detail. Then, thermal cycle and vibration analyses are carried out and optimized by finite element simulations in Section 3. Finally, the performance and feasibility of the optical transceiver module are evaluated in Section 4.

2. Design and fabrication of the organic optical bench

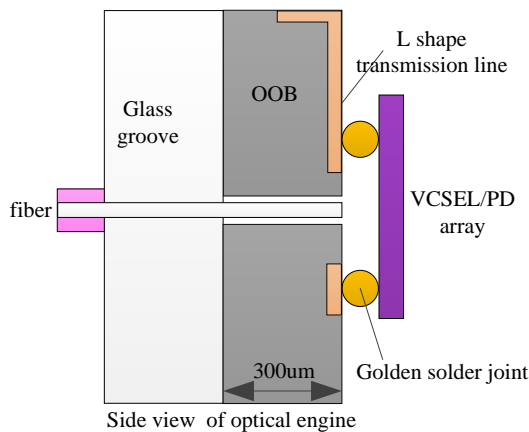The proposed optical engine based on organic optical bench is shown in Fig. 1.

Fig 1. Proposed optical engine structure based

on organic optical bench (color online)

In our structure, the optical chips including VCSEL array and PD array are flip-chip mounted on the organic substrate by golden balls. There are 12 through-holes on the organic substrate, the spacing of which is consistent with the adjacent channel spacing of the optical chips. The through-holes are fabricated on OOB to facilitate aligning of optical fibers to realize direct optical coupling without lens between fiber and optical chips. The array with 12 optical fibers is fixed through the glass v-grooves. And the fibers are designed with a bare segment of 300um outside the glass v-grooves which is consistent with the thickness of the organic substrate. "L" shape transmission line on the OOB is designed for electrical interconnection to PCB board via bonding wires.

To evaluate the performance of the optical subassembly, optical simulations on coupling efficiency and misalignment tolerance are very critical since they have a great impact on the output/input power of the module. The simulations are performed by beam propagation method (BPM), and the results are shown in Fig. 2. According to the simulation results, the -1dB misalignment tolerances of for 10 Gbps VCSELs and

PDs in X/Y axis are ±20μm and ±18μm, respectively. And the -1dB misalignment tolerances of for 25Gbps VCSELs and PDs in X/Y axis are ±20μm and ±10μm, respectively. The 25Gbps PDs has smaller photosensitive surface than 10Gbps PDs so the misalignment is much smaller. The misalignment tolerance shows the optical engine can be used for high speed VCSEL and PD array.
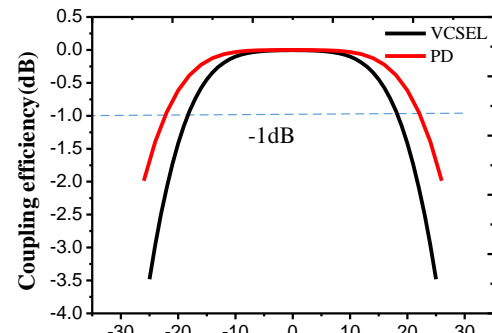
(a) X/Y -1dB tolerance (μm) for 10Gbps VCSEL and PD
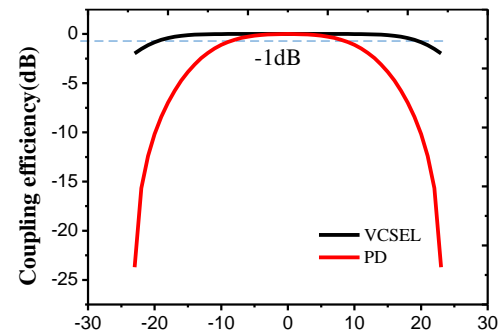
(b) X/Y -1dB tolerance (μm) for 25Gbps VCSEL and PD

Fig. 2. Optical coupling efficiency with the variation of X/Y axis (X is the length direction of the organic substrate; Y is height direction of the organic substrate) (color online)

The overall bandwidth of the optical engine is decided by loss of electrical path, optical coupling efficiency, and inherent bandwidth of the chips. Thanks to the high coupling efficiency and large misalignment tolerances of the optical engine, optical coupling loss has minor influence on bandwidth. For the chips employed in the module, bandwidth of optical chips (VCSEL/PD) are both beyond 10Ghz, and electrical chips (Driver/ TIA) also support up to 14Gbps data rate. Therefore, neither optical coupling efficiency nor inherent bandwidth of the chips is the main factor limiting the bandwidth of the optical engine.

The electrical path on OOB comprised of bonding wires and short transmission line is simulated and optimized by the 3-D electromagnetic simulation software Ansys HFSS. In order to evaluate the respective effects of bonding wire and transmission line on bandwidth, we have simulated the forward transfer coefficient (S21) of the path at different length of bonding wire and compared the loss with traditional optical engine which is realized by direct wire bonding

between VCSEL/PD and driver/TIA as shown in Fig. 3. The simulation results show that 3-dB bandwidth of the electrical path decreases as length of bonding wire increases, and the bandwidth of the L-shaped transmission line structure (WB+TL) we propose is only slightly smaller than the traditional structure (WB only). At the frequency of 20GHz, the loss of L-shaped transmission line (WB+TL) and direct wire bonding (WB only) with the same 600um golden wire is 2.5dB and 2.3dB respectively, which means loss caused by short transmission line on organic substrate is only 0.2dB. And as frequency increases, this value remains almost the same. In addition, at the frequency of 20GHz, the loss of L-shaped transmission line (WB+TL) increases from 1.6dB to 3.1dB when the length of golden wire increases from 400um to 700um. Therefore, the bandwidth of electrical path on OOB is mainly determined by the length of bonding wire. However, in our design, as seen from Fig. 3, even though the length of golden wire is long as 700um, 3-dB bandwidth of the electrical path on OOB can reach 20GHz. During design and assembly, we have struggled for minimizing the length of golden wire as much as possible to increase bandwidth, for example, reducing the height difference between OOB and PCB board (approximately 70um), and shortening the distance from OOB to PCB (nearly 200um), which makes the actual length of golden wire is no more than 500um.
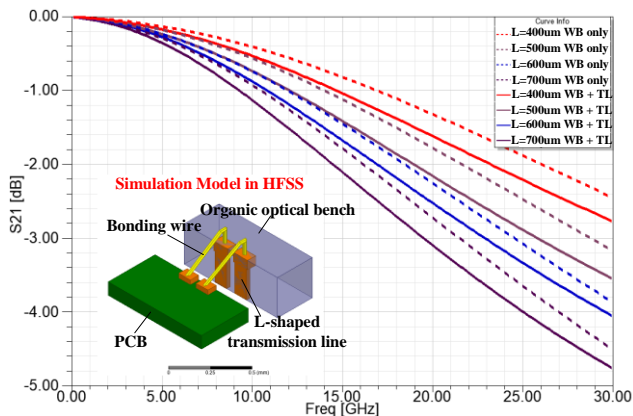

Fig. 3. Modeling and simulation of electrical path on the organic optical bench (OOB) (color online)

The fabrication process of the proposed OOB is illustrated in Fig. 4，which includes the fabrication of fiber guide holes, bonding pads, and 90°-bend microstrip lines shaped like "L". 400mm×250mm BT HL832NSF type LCA substrate [8] with peeling able ultra-thin double side copper foil is chosen as temporary core layer. Firstly, photolithography is utilized to form photoresist (PR) patterns which will enable copper etching at specific positions on the organic substrate, as a result, transmission line can be etched on both side of core layer (I). Secondly, copper bumping is fabricated by electroplating on both side for "L" interconnection (II). Then, A BT prepreg (PP) is pressed on both side of the

BT core layer as dielectric (III). After that, the temporary core is peeled off from the released film interface (IV). And copper foil etching is following (V). Next, through-holes which will act as fiber guide holes are fabricated by mechanical drill method. Furthermore, copper bumping is split into two parts by through-holes to form side pads (VI). At last, electro-less nickel electro-less palladium immersion gold (ENEPIG) is carried out by chemical plating for reliable wire bonding and flip chip (VII).
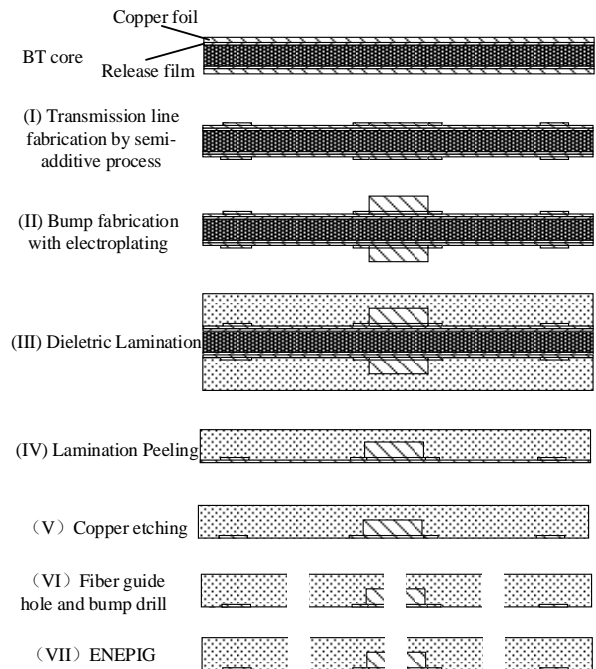

Fig. 4. The fabrication process of the OOB

The fabricated OOB is shown in Fig. 5. The 90° "L" shape transmission line to achieve electrical bending interconnection is embedded in the material and only the surface is exposed to air decided by the afore-mentioned fabrication process. To ensure the strength of golden wire, a wire bonding test is carried on. Results shows that pull force of golden wire is about 7-10g/N, which verifies the ENEPIG surface treatment is satisfying. Fiber guide holes are measured with diameter of 135um±5um which can support fiber alignment within optical coupling tolerance.
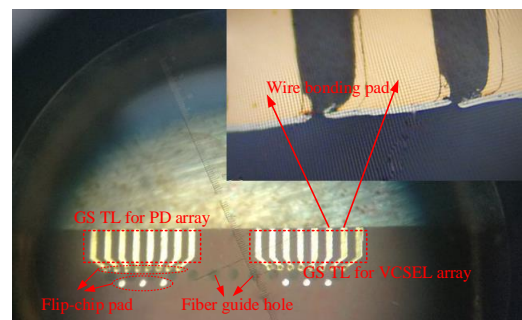

Fig. 5. Photo of the OOB (color online)

3. Thermo-mechanical and vibration analysis of the optical engine

3.1. Material properties test

Characteristic of organic substrate material is significant which may affect the optical coupling efficiency and reliability of module. Prior to simulation and modeling, thermo-mechanical properties of BT laminate are characterized by Dynamic Mechanical Analyzer (DMA) and Thermal Mechanical Analyzer (TMA). Fig. 6 illustrates the storage modulus, loss modulus, and tan delta of the BT laminate dependent on temperature at a frequency of 1 Hz. As temperature increases, storage modulus gradually decreases. And storage modulus decreases dramatically at glass transition region. When temperature is higher than glass transition temperature (Tg), storage modulus is a small value and keeps decreasing. On the contrast, loss modulus and tan delta of the BT laminate increases firstly with temperature and reach their peak value at the glass transition temperature. Generally, the temperature corresponding to the maximum value of tan delta at 1 Hz is defined as Tg of material [9]. Tg of the BT laminate is up to 275°C as shown in Fig. 6, which is much higher than most other organic materials.
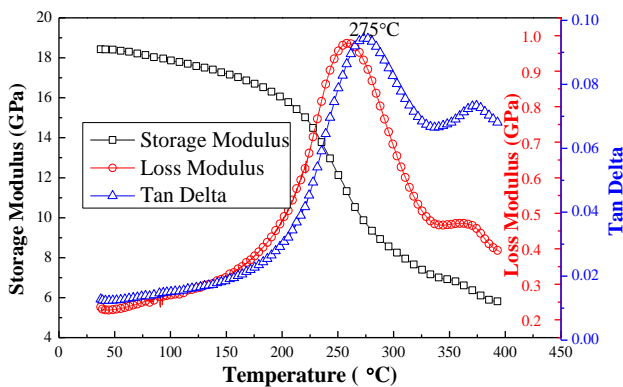

Fig. 6. Dynamic mechanical performance of the BT laminate at a frequency of 1 Hz (color online)
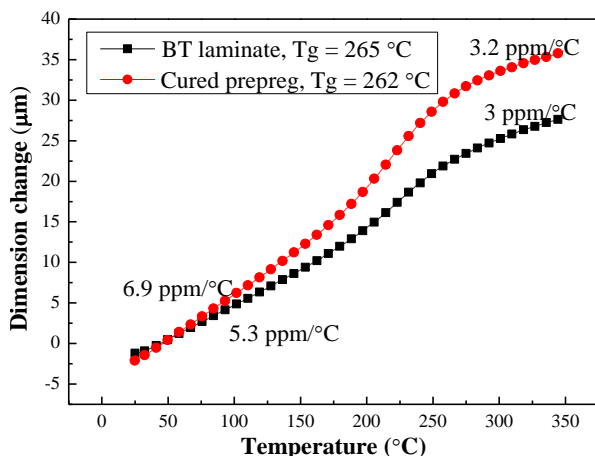

Fig. 7. Comparison of Tg and in-plane CTE between cured prepreg and BT laminate (color online)

Fig. 7 illustrates comparison of Tg and in-plane coefficient of thermal expansion (CTE) between two kinds of laminated materials named BT laminate and cured prepreg. It can be found that Tg of BT laminate and cured prepreg is of little difference, which is 265 °C and 262 °C respectively. And Tg of BT laminate is very close to the value tested by DMA. In-plane CTE of the BT laminate at the temperature above Tg is lower than that below Tg, which is about 3 ppm/°C and 5.3 ppm/°C respectively. When temperature is below Tg, in-plane CTE (5.3 ppm/°C) is nearly same with CTE of VCSEL (5.73 ppm/°C) and PD (5.73 ppm/°C) which means that CTE of OOB is well matched.

3.2 Thermo-mechanical analysis of the optical engine

The size of the OOB, the VCSEL array and the PD array is 0.3mm×5.56mm×1.32mm, 985um×285um×150um and 985um×285um×150um respectively. Golden solder ball joints between optical devices and organic substrate not only function as electrical connections, but also as mechanical supports. The temperature changing is equivalent to the temperature load on the golden joints. The thermal expansion coefficient of various materials will produce internal stress, so the solder joint between the device and the substrate will undergo repeated stress under the cyclic thermal load, resulting in the failure of the solder joint. The strain will influence optical coupling efficiency at the same time.

An approximate ideal model to simulate the actual structure is established by Ansys Workbench based on the method of finite element modeling. Due to the complexity of the proposed structure, the simulation model needs some necessary simplifications. Firstly, since the size of pads on the optical and electrical chips and metal lines on the organic substrate is considerably small relative to the module size, they can be ignorable when setting up model of the structure. Besides, since the transmitter (VCSELs) and receiver (PDs) parts in the proposed structure are centrosymmetric, we can only take solder joints between emitting part and substrate as a representative to study their reliability. Emitting part of the proposed structure consists of a 1 × 4 VCSEL array which has 11 pads, so a corresponding number of gold balls are needed to modeling actual structure.

The thermo-mechanical properties of the materials used in the simulation are listed in Table 1.

Table 1. Thermo-mechanical properties of materials

Component	Materials	CTE (°C/ppm)	Poisson Ratio	Young's modulus（Gpa）
VCSEL	GaAs	5.73	0.31	85.5
PD	GaAs	5.73	0.31	85.5
Solder ball	Au	14.4	0.42	77.2
Organic optical bench	HL832NSF type LCA	$\alpha1 = 6.9, \alpha2 = 3.2$	0.18	34
Fiber	SiO2	13	0.17	67
Groove	Glass	7.2	0.208	72.9
Copper	Cu	16.4	0.343	110

Under cyclic temperature loading, the maximum equivalent stress variation at solder joints is as shown in Fig.8. To verify the applicability of our proposed structure under wide temperature range, the temperature in simulation is chosen to vary from -55℃ to 70℃. When the temperature drops to -55 ℃, there is obviously a large temperature change compared with the ambient temperature of 25℃, so thermal stress caused by shrinkage and deformation of optical device and organic substrate is the largest at -55℃. Fig. 9 shows the distribution of the maximum stress and strain.

The simulation results show that thermal stress distribution is almost uniform for each golden solder joint. And the thermal stress concentrates mainly on the contact surface of the solder joint between organic substrate and optical device pins. For a single solder joint, the thermal stress on its edge is the greatest. The strain distribution of a solder joint corresponds to the thermal stress distribution, and the strain is small enough to be ignored. The maximum stress of solder joint is about 150 MPA, and the yield strength of golden ball at 25 ℃ and 250 ℃ is 200 MPA and 227 MPA respectively. Therefore, the golden solder joints between optical chips and organic substrate have been in the elastic strain stage, and the stress and strain will change periodically without plastic strain.
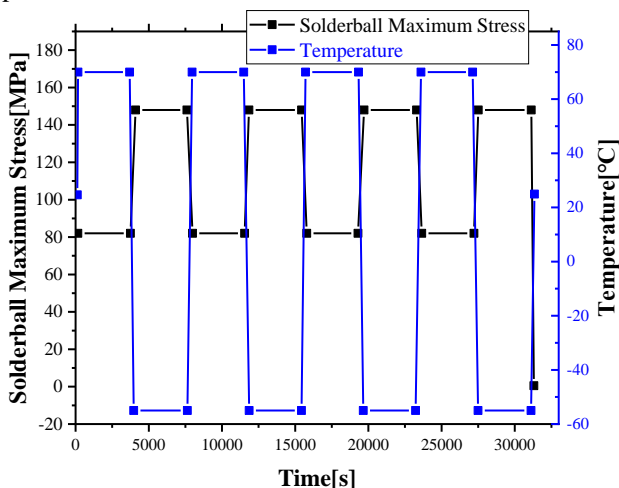

Fig. 8. Temperature variation and golden solder stress (color
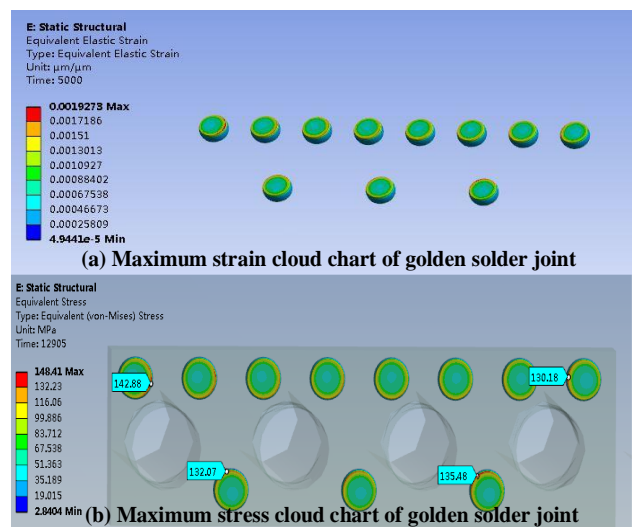
online)

(a) Maximum strain cloud chart of golden solder joint

(b) Maximum stress cloud chart of golden solder joint

Fig. 9. Strain and stress cloud chart of golden solder joints

between VCSELs and organic substrate (color online)

For optoelectronic application, the optical coupling efficiency is one of the key indexes that determine the performance of the modules. Therefore, the optical coupling efficiency of the proposed structure is analyzed under the condition of thermal cycling loading. Taking the transmitter as an example, the relative displacement of the fiber array and the VCSEL array under thermal cycling are compared with their coupling tolerances. Since the position of the optical fiber array (FA) is fixed by the glass V groove, the displacement of the glass V groove and the optical fiber array can be considered as a entirety. The displacement cloud image of VCSEL and glass V groove in the direction of X, Y and Z is shown in Fig. 10. X is the length direction of the organic substrate, Y is height direction of the organic substrate and Z is the thickness direction which indicates the direction of the straight hole in the vertical organic substrate.

It can be found that the displacement direction of VCSEL array is consistent with glass V-groove. Under the condition of thermal cycling, the curves of node displacement at the central position of VCSEL array with time can be obtained. For the glass V-groove, the node

displacement relative to the central position of the VCSEL array can be selected. The node displacement can be regarded as the central displacement of the fiber array, and the curves of the central displacement of the fiber array related to time can also be obtained. Comparing the displacement of two nodes in the same coordinate system, it can be found that the maximum relative displacement of fiber array and VCSEL array in X and Y direction is 0.6 um, and 1.3 um respectively. The maximum relative displacement in Z direction between fiber array and the VCSEL array is almost zero. By comparing the above results with the 1dB alignment tolerance of the proposed structure, we found that relative displacement of the VCSEL array and the fiber array has little effect on the optical coupling efficiency under the thermal cycling condition.
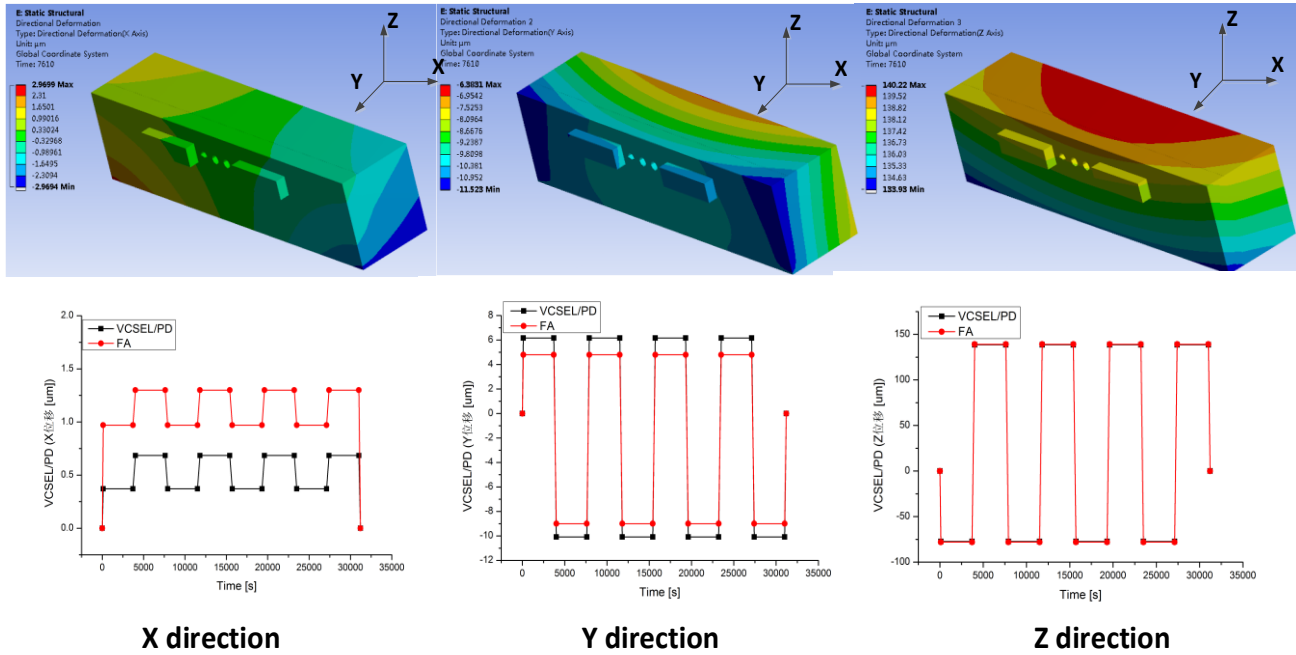

X direction   **Y direction**   **Z direction**

Fig. 10. The displacement cloud image of VCSEL and glass V groove in the direction of X, Y and Z (color online)

3.3. Vibration analysis

For optical modules, in addition to thermal shock will affect the reliability of the product, vibration shock is also one of the important factors affecting reliability. The reliability of golden solder joints on organic substrates should be studied in random vibration environment.

Table 2. Mode analysis

Mode	Frequency (Hz)
1	680.87
2	2409
3	4245.5
4	6386.4
5	7740.7
6	9416.2

Before performing random vibration analysis, the modal and characteristic frequency of the structure should be determined. The modal is the vibration characteristic of the structure itself, which is determined by the material and form of the structure and has nothing to do with external environmental factors. In eigenmode analysis, the model adopts the same structure as that used in thermal cycle analysis. The modal analysis of the structure is carried out and the sixth resonance mode is extracted, as shown in Table 2. It can be seen from the table that the natural frequencies of each resonance are quite different and there is no multi-order resonance.

First of all, acceleration power spectrum is calculated. The power spectral density is lower than 2000 Hz. Comparing the multi- resonance mode frequency, it can be found that the first resonance mode frequency has a great influence on the whole structure. The equivalent stress distribution of golden solder joints on organic substrate is shown in Fig. 11. Through the analysis of solder joints, it can be found that the stress and strain of the solder joints on the outer side of organic substrates are relatively large, and the stress and strain of the inner solder joints decrease gradually. The maximum 1 σ stress point is 0.6 MPa and the yield strength of the solder joint is 220 MPa, so the elastic strain and the non-plastic strain will occur in the solder joints. The above results show that there is no damage to the solder joints under random vibration conditions, and the vibration resistance and environmental adaptability of solder joints are fine.
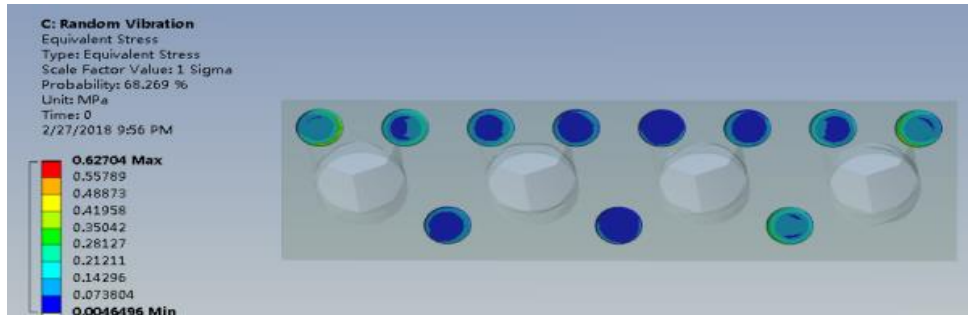
Fig. 11. Equivalent stress distribution of golden solder joints (color online)

The optical coupling efficiency of the structure is analyzed under the condition of random vibration loading, too.
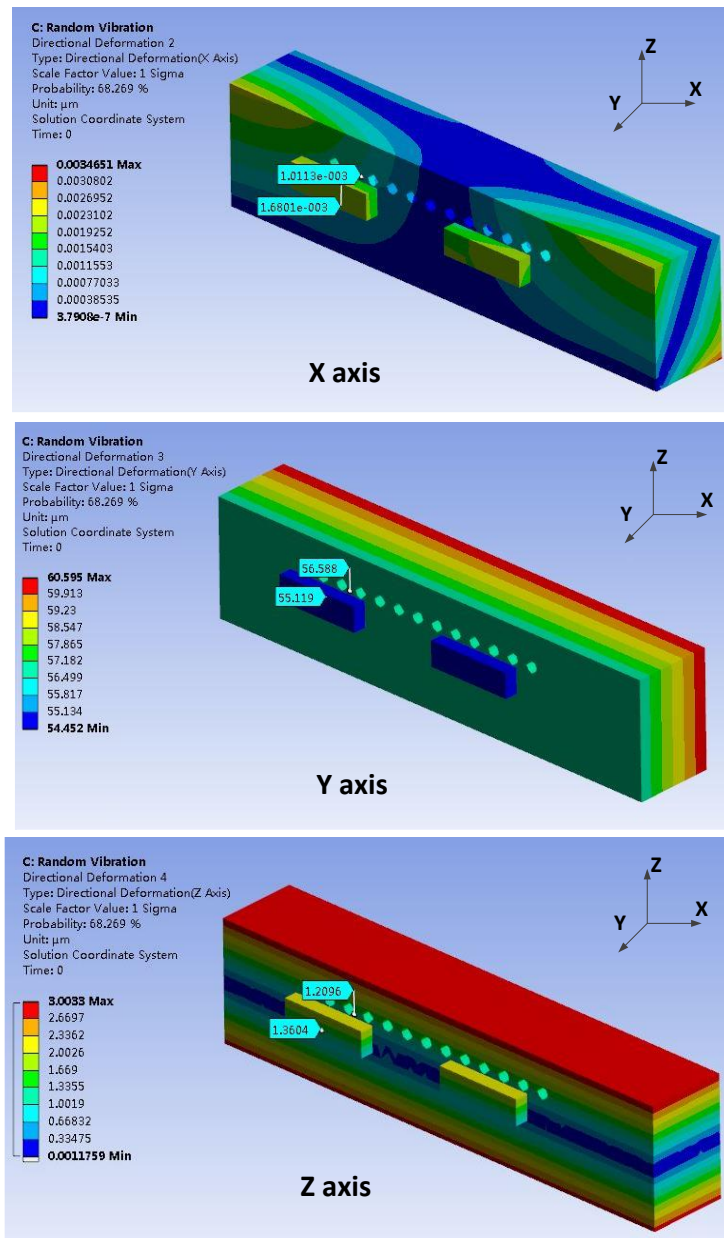

Fig. 12. The relative displacement of the glass V-groove and the VCSEL array (color online)

Taking the transmitter part as an example, the displacement of fiber array and laser under random vibration is compared. In the same way, the relative displacement of the glass V-groove and the VCSEL array is compared, as shown in Fig. 12 in the way of displacement cloud diagram of the VCSEL and the glass V-trough in the direction of X,Y,Z. Comparing the node displacement of the central position of VCSEL array with the node displacement on the glass V-slot opposite the central position of the VCSEL array, it can be seen that the relative displacement of the fiber array and the VCSEL array in the X, Y and Z direction is nearly zero, 1.4 um and 0.1 um respectively. By comparing the above results with the 1 dB alignment tolerance of the structure, it can be seen that the relative displacement of the VCSEL array and the fiber array has so little effect on the optical coupling efficiency under random vibration conditions that it can be neglected.

4. Assembly and performance test

To verify feasibility of the proposed optical engine based on OOB, an OSA is assembled consisting of OOB, optical chips, electrical components, fiber array, test board etc. The assembly process of the module is relatively convenient and cost effective. Firstly, the optical chips including VCSELs and PDs are mounted on the fabricated OOB with a high-precision flip-chip bonder (Fig. 13(a)). Then, the bare parts of 12-channel array fibers with diameter of 125um are inserted into the OOB through the fiber guide holes with the same spacing of 250um. In addition, UV curable epoxy is used to cover and fix the fibers, thus increase stability of optical performance (Fig. 13(c)). Simultaneously, electrical components including drivers, TIAs, and other passive devices are mounted on the electrical PCB by surface mounting technology (SMT). Then, the prepared optical subassembly and the assembled electrical PCB are attached together on a large copper plate by the UV curable epoxy. And electrical interconnection is completed between optical chips and electrical chips by wire bonding (Fig. 13(d)).
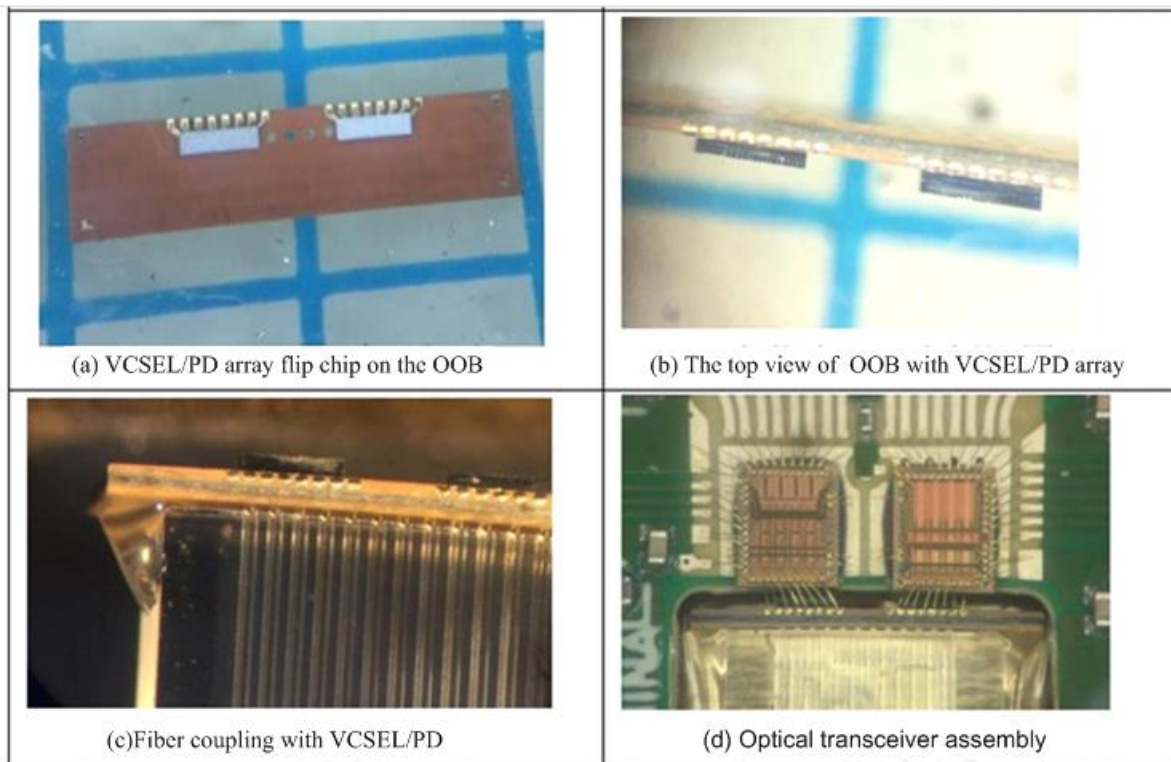

(a) VCSEL/PD array flip chip on the OOB

(b) The top view of OOB with VCSEL/PD array

(c)Fiber coupling with VCSEL/PD

(d) Optical transceiver assembly

Fig. 13. Optical coupling engine assembly (color online)

The eye diagrams operating at 10Gbps are evaluated to verify performances of our structure. Fig. 14 shows the 4-channel eye diagrams of the transmitter. The extinction ratio of all four transmitters is greater than 4dB, and the optical eye is open enough to support standard 10Gbps optical eye mask.

Fig. 15 shows the eye diagrams of the receiver. The 4-channel eye diagrams at 10Gbps are also clearly open. Muti-channel 25Gbps has not been tested limited to high speed test board.
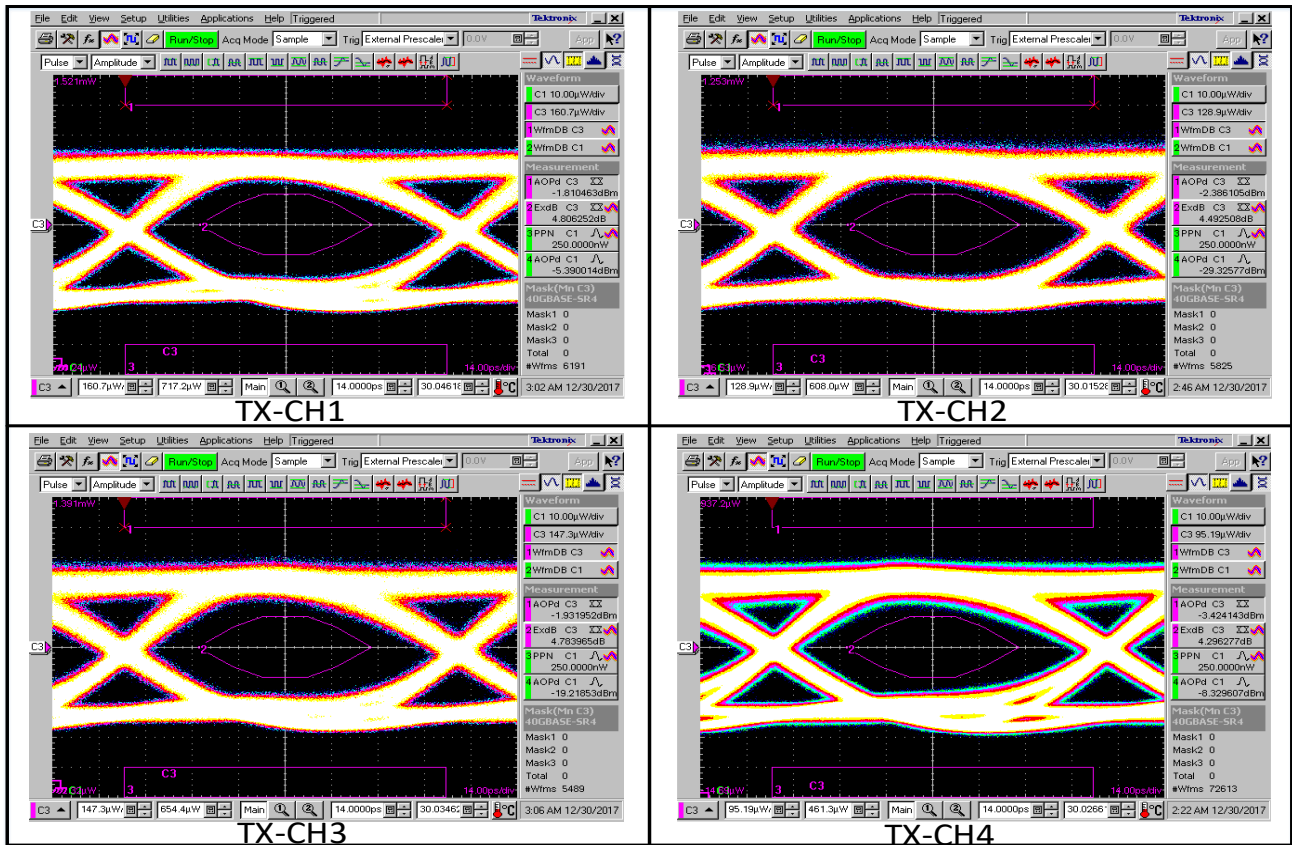
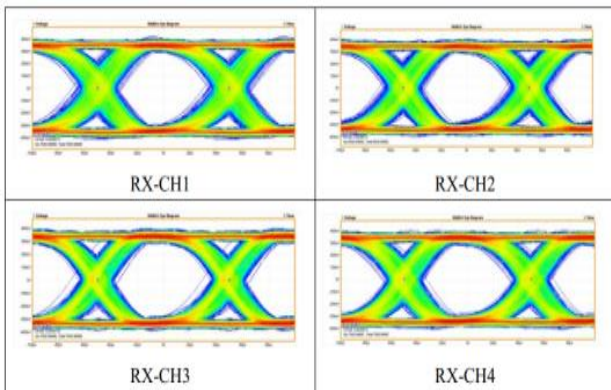*Fig. 14. Eye diagram of 4-channel transmitter at 4×10Gbps (color online)*

Fig. 15. Eye diagram of 4-channel receiver
at 4×10Gbps (color online)

5. Conclusion

In this paper, a low-cost and small-scale optical engine based on organic substrate is proposed. The design and fabrication of the structure is introduced firstly. Then material thermal-mechanical property of organic substrate is tested and thermal cycle and vibration analysis of the structure is carried out. The simulation results show that stress, strain and vibration have little effect on the coupling efficiency and golden bump joint has good reliability. Finally, the optical engine is assembled to verify its feasibility and availability. The test results demonstrate that the optical engine can be applied in short-reach optical interconnection and high-speed application such as video/audio signals transmission.

References

[1] https://thunderbolttechnology.net/product/plugable-08m-40gbps-thunderbolt-3-cable-08m-100w-charging.
[2] Jerry Gao, Hengju Cheng, Hui-Chin Wu et al., Journal of Lightwave Technology **35**(15), 3125 (2017).
[3] Chaerin Hong, Seung-Hoon Kim, Sangmo Cha, Sung Min Park, IEEE Photonics Journal **11**(2), 6601011 (2019).
[4] Mathieu Charbonneau-Lefort, Michael J. Yadlowsky, Journal of Lightwave Technology

33(4), 872 (2015).

[5] Chin-Ta Chen, Hsu-Liang Hsiao, Po-Kuan Shen et al., Optical Engineering **51**(11), 115005 (2012).

[6] Ning-Ning Feng, Xiaochen Sun, Journal of Lightwave Technology **33**(4), 811 (2015).

[7] Kisung Park, Gil Dong Lee, Sang No Lee et al., 2017 European Conference on Optical Communication (ECOC), p. 1.

[8] Sumy Mathew, Tilo Welker, Nam Gutzeit et al., 2017 47th European Microwave Conference (EuMC), p. 624.

[9] Teng Li, Gonzalo Guelbenzu, Chenhui Li et al., 2017 IEEE 67th Electronic Components and Technology Conference, p. 1755.

[10] Hideyuki Nasu, Kazuya Nagashima, Yozo Ishikawa et al., 2016 IEEE CPMT Symposium Japan (ICSJ), p. 31.

_____

[*]Corresponding authors: liufengman@ime.ac.cn
                                     xuehaiyun@ime.ac.cn